Research Article

Simulation based testing and performance investigation of induction motor drives using matlab simulink

Kehinde Adeleye Makinde[1] · Mutiu Shola Bakare[2] · Benjamin Olabisi Akinloye[3] · Abraham Olatide Amole[4] · Oludamilare Bode Adewuyi[5] · Uthman Oluwatosin Zubair[6] · Waheed Olaide Owonikoko[7]

Abstract

Induction motors (IMs) are the most widely employed electrical motors due to their robust construction and adaptability. Due to their versatility and wide range of applications, it is crucial to examine the performance of these motors using a simple but thorough simulation model. In this study, we present the simulation models to conduct the DC test, the no-load test, and the locked rotor test on a three-phase induction motor using MATLAB/Simulink. These three tests are fundamental to determining the characteristics of a three-phase induction motor equivalent circuit. Furthermore, the authors extend the model to determine the starting current, starting torque, and breakdown torque of the motors under inquiry. The research further employs the right code in the MATLAB environment to ascertain the motors' torque-speed and current-speed properties. The results of the simulations are found to closely match the values achieved in real trials. Hence, this model can be employed to enhance teaching and research in the field of electrical machinery.

Article Highlights

- This paper explains a computerized procedure employing MATLAB software to carry out vital tests on induction motors. The research shows that using the methods described in this paper, induction motors can be safely tested for their operating characteristics.
- The benefit of the computerized methodology described in this paper is that it provides a modelling tool and methodology to expand research on induction motors with high accuracy and reliability.
- The numerical method developed in this article is a suitable tool in teaching and education.
- Beyond the three common tests (dc test, no-load test and locked rotor test) to determine the equivalent circuit of induction motors, this paper further extends the research to use the simulation models to determine the starting current, starting torque and the breakdown torque of an induction motor as well as its torque-speed and current-speed characteristics.

✉ Mutiu Shola Bakare, Shola.bakare@studwc.kiu.ac.ug; Oludamilare Bode Adewuyi, adewuyiobode@gmail.com | [1]School of Computing, Engineering and Digital Technologies, Teesside University, Middleborough, UK. [2]Department of Electrical Engineering, Kampala International University, Kampala, Uganda. [3]Department of Electrical and Electronic Engineering, Federal University of Petroleum Resources, Effurum 333116, Delta, Nigeria. [4]Department of Electrical, Electronics and Computer Engineering, Bells University of Technology, Ota, Ogun State, Nigeria. [5]Department of Electrical and Electronic Engineering, First Technical University, Ibadan 200255, Nigeria. [6]Department of Electrical and Electronics Engineering, Eastern Mediterranean University, Famagusta, Cyprus. [7]Department of Electrical and Biomedical Engineering, University of Vermont, Burlington, VT, USA.

1 Introduction

Induction motors (IMs), the most widely used electrical motors, are renowned for their dependability, affordability, sleek form, and robust construction. Furthermore, because to developments in power electronics and microprocessor technology, high-speed IMs powered by variable frequency provide a number of advantages in terms of durability, little maintenance, low cost, craftwork, and other aspects [1, 2]. The specifications for testing synchronous and induction devices are detailed in great depth in [3]. Given that the majority of electrical equipment are powered at the required frequencies, it is customary for testing methods to be constructed around a fixed-frequency power source, often 50 or 60 Hz. But as inverter-compatible IMs become more prevalent, they are no longer restricted to 50 or 60-Hz power. Unless they are evaluated at 50 or 60 Hz, which does not provide the essential operational information, such devices cannot work at higher frequencies. It is crucial to build and interpret computer models and simulations of induction motors in order to investigate the dynamic state and steady state operations of the motor under various loading scenarios. Additionally, the virtual tests have no restrictions on the test duration, iteration, measuring instruments, or test rigs. They completely sidestep the issues associated with destructive tests like the load test and breakdown torque test. These tests are thus entirely cost-effective.

It is also important that modeling and numerical tools be developed for experiments involving induction machines to serve as valuable preliminary exercises before students carry out the main laboratory experiments. This is because, in majority of educational institutions, experiments that involve significantly big machines and complex measurements are often sidelined and left undone as compared with those that make use of smaller equipments and simple measurements. In addition, it is expected that students cover as many experiments as possible within limited timescale in the laboratory. These include setting up the test rigs, carrying out at least three induction motor experiments, taking measurements, investigating performance under varying loads- usually within two hours. This time constraint often results in students rushing through the lab sections thereby preventing them from valuing the operations of the induction machines and understanding the knowledge the experiments are designed to achieve.

Examining motor losses may often be done under three different ideal situations: no load, high load, locked rotor, and iron loss perturbation [4]. These situations include ideal no load, excessive load, locked rotor, and

iron loss disturbance. The extensive body of research on the usage of IMs in industries like rail [5], pumps [6], etc. provides proof of their value. In order to reduce unneeded harm and prospective losses, software simulation studies make it feasible to realistically assess a system. As a result, the literature often references simulated IM experiments. For instance, while implementing Indirect Field Oriented Control (IFOC) of three-phase IM in the PSIM environment, the five levels of the incremental system have been considered [7]. Direct torque control of IM was employed in a simulation research that combined motor parameter-dependent and motor parameter-independent optimization approaches [8]. By simulating and duplicating the dynamic processes that occur during the first launch of high-speed IMs [9]. It has been shown that the created model has the capacity to precisely predict the characteristic of IMs by comparing the simulation and experimental data. According to a recent research, a smartphone may infer the IM frequency from mechanical vibrations and motor sounds. The application, dependability, and accuracy of the smartphone-based approach have been shown by the experimental findings published in the paper [10].

The control of a number of variables, including current, torque, and speed, is crucial for ensuring its best performance and integrity [11–13]. Direct field-oriented control (DFOC) [14], H-infinity method [11], sliding mode control [15], non-vector control [16], resonant control [17], field-oriented control(FOC) [13], and model predictive control (MPC) [18] are just a few of the control methods that have been used to regulate a number of IM parameters. The study on adaptive fuzzy based model predictive torque control for IM ripple attenuation [19], for example, demonstrates how well accepted MPC are. The control method was shown to be effective for real-time torque and flux control via simulation and hardware-in-loop testing on a 1.1 kW IM. Similar to this, a rotor flux-oriented nonlinear MPC of IM has been considered [20], and it has shown outstanding controlled variable performance under typical operating conditions, load disturbances, parametric condition, and at a low rotor speed. Model predictive torque control of IMs for current ripple reduction was also explored in the work of [21]. The effects of current total harmonic distortion and electrical power consumption are reflected in the 5.5 kW IM dSPACE-controlled simulation, which is based on MATLAB/Simulink. In a comparison of MPC and direct torque control (DTC), it was discovered that the latter chooses the proper voltage vector, which is crucial for the optimal control performance.

Sensorless control technology has lately achieved significant advancements in the control of IM with the development of the quadrature model reference adaptive system (Q-MRAS), upgraded (Q-MRAS), and neural network

for the management of instantaneous reactive power, speed, and torque [22–24]. Like all systems, IMs are prone to faults; however, techniques for fault-tolerant control of IMs have been developed using a variety of methods, including modified rotor flux estimators [14], virtual current sensor (VCS), wavelet index based boosted model reference adaptive system (BMRAS) [24] and CB-MRAS [25]. The work of [26]created an automated fault-tolerant control (AFTC) mechanism by using the built-in fault tolerance and self-derating approach. A six-phase IM was used to demonstrate the effectiveness of the developed AFTC's simplicity and reliability in controlling multiphase IMs. However, little effort has been made to determine factors like the starting current, starting torque, and breakdown torque. Some of the information that has been published so far has taken into consideration doing dc testing, no-load tests, and locked-rotor tests.

The goal of this study is to examine the performance of IM using a simple but thorough simulation model employing simulation models in the MATLAB/Simulink environment. The study is distinctive in that it looks at the performance characteristics of the motors under consideration as well as doing tests to gauge the starting current, starting torque, and breakdown torque. The remainder of the study is divided into the following sections: Sect. 2 covers the theoretical foundations of induction motor testing. Section 3 provides the simulation designs for various tests, and Sect. 4 concludes the study.

1.1 Relevance of the study

The proliferation of affordable personal computers and low-cost software packages makes computer-assisted training tools an integral part of both lecture classes and lab experiments in electrical engineering studies. The computerised models of induction motors developed in this paper will assist the lecture classes by facilitating the tutor, through the computer-produced visuals, to demonstrate effortlessly various tests necessary to determine the operating characteristics of induction motors as well

as the motor's performance when subjected to different levels of load.

Combining software simulation approach as discussed in this paper with laboratory works augments the students' as well as researchers' laboratory experience by offering the chance to validate the findings of laboratory studies and link them with the results from computer models. Such a comparative study propels learners to fully understand the limits of hardware experiments thereby appreciating that modelling alone cannot completely replace the real-life experiments due to some omissions and assumptions in the computer models.

Hence, this paper will serve as a useful model for researchers in electrical machine to fully understand the operation of induction motors. Similar experiment has been conducted in [27] where the authors used computer models and lab experiments to verify the three tests- dc-test, no load, and blocked rotor tests. The results clearly showed that the Simulink models can be used to correctly carry out these tests without the need for the real-time experiments. This paper further extends the model to perform the starting torque test, starting current test and to plot the torque-speed as well as the current-speed characteristics of an induction motor.

2 Materials and methods: different tests on three-phase induction motor

Experiments such as the DC test, the No-load test, and the Lock rotor test are often carried out to determine the characteristics of the per-phase equivalent circuit of a three-phase IM of Fig. 1.

2.1 DC test

The dc test is used to determine the stator resistance R_1 Value. Applying dc voltage to the stator winding causes a dc current to flow across the stator winding, which results in zero motor reactance and no voltage being produced in

Fig. 1 Per-phase equivalent circuit of a 3-phase Induction Motor
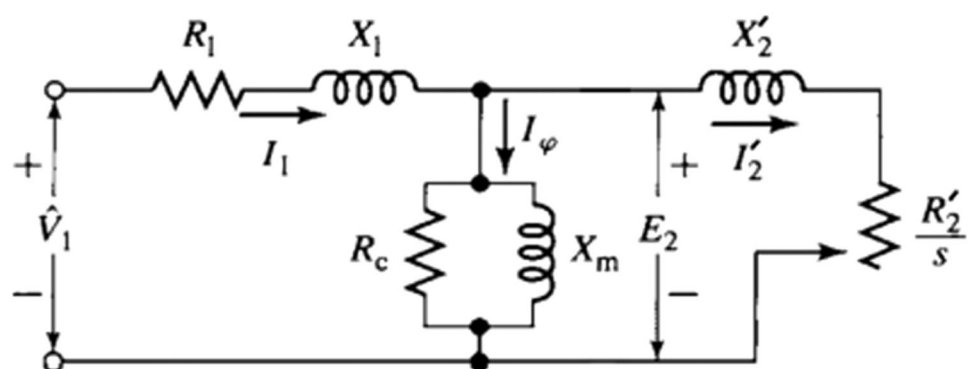
the rotor circuit. The stator resistance is the sole component of the circuit that blocks current flow. This test is done on an isolated motor to test the resistance of the stator windings. To get an accurate measurement, a low-reading ohmmeter or a high-resolution digital multimeter are needed. The results obtained from the DC test are approximations [28, 29]. The stator resistance may therefore be computed as follows:

$$R_1 = 0.5\frac{V_{dc}}{I_{dc}} \tag{1}$$

2.2 No-load test

The no load test on an IMs is the same as the open circuit test on a transformer. It provides data on rotational losses and exciting current. The machine is evaluated as a motor with no associated load at rated voltage and stator winding at rated frequency [30]. The DC resistance test is performed to assess the resistance of a stator by passing an appropriate direct current through it and measuring the voltage drop between the terminals. The test offers a check for the computed results or a foundation for predicting efficiency when done with the motor cool (at room temperature) [28, 29].

A no-load test is used to determine the core resistance value R_c and the magnetizing reactance X_m in the IM per-phase equivalent circuit. While the motor shaft is not connected to any loads, the stator winding is subjected to the test's maximum voltage and frequency. The three phase input power, line-line voltage, and phase current may then be calculated. At no-load, the rotor rotates at approximately the synchronous speed N_s and thus, the slip $s \approx 0$. Therefore, the reflected rotor resistance $\frac{R'_2}{s} \approx \infty$ and $I_2 \approx 0$.

The power equation for the circuit in complex form is given by:

$$S_{nl=}I_{nl}^2 R_1 + (I_{nl}\cos\emptyset_{nl})^2 R_c + j(I_{nl}^2 X_1 + (I_{nl}\sin\emptyset_{nl})^2 X_m \tag{2}$$

where S_{nl} is the apparent power at no-load, $\emptyset_{nl}$ is the power angle at no-load. Assuming the equivalent resistance R_{nl} and reactance X_{nl} are in parallel (since $R_c \gg R_1$ and $X_m \gg X_s$), then:

$$S_{nl} = (I_{nl}\cos\emptyset_{nl})^2 R_{nl} + j(I_{nl}\sin\emptyset_{nl})^2 X_{nl} \tag{3}$$

From (2) and (3), the core loss resistance R_c and the magnetizing inductance X_m can be expressed as:

$$R_c = R_{nl} - \frac{R_1}{\cos^2\emptyset_{nl}} \quad \text{and} \quad X_m = X_{nl} - \frac{X_1}{\sin^2\emptyset_{nl}} \tag{4}$$

where R_{nl} and X_{nl} are given as:

Table 1 X_1 and X'_2 Versus rotor class and X_{lr}

Rotor class	X_1	X'_2
Design A class	$0.5X_{lr}$	$0.5X_{lr}$
Design B class	$0.4X_{lr}$	$0.6X_{lr}$
Design C class	$0.3X_{lr}$	$0.7X_{lr}$
Dn D class	$0.5X_{lr}$	$0.5X_{lr}$

$$R_{nl} = \frac{P_{nl}}{3(I_{nl}\cos\emptyset_{nl})^2}; \quad X_{nl} = \frac{Q_{nl}}{3(I_{nl}\sin\emptyset_{nl})^2} \tag{5}$$

X_1 is obtained from locked rotor test while R_1 is obtained from the dc test.

2.3 Locked rotor test

A locked rotor test is performed to determine the rotor resistance R'_2 and the total of the leakage reactance X_1 and X'_2. The rotor is locked during the test to prevent it from spinning, and to keep the current within the limit, the supply voltage is gradually raised from a low amount until the rated current is reached. The motor input is then used to measure the three-phase active power P_{lr}, reactive power Q_{lr}, line-to-line voltage V_{lr}, and phase current I_{lr}. This test is conducted at a test frequency that is generally lower than the stated operating frequency [31, 32] in order to correctly assess the rotor resistance in certain design-type IMs. The slip equals 1, which results in a low rotor impedance and causes the rotor current to be larger than the magnetizing current since the rotor is stuck and unable to spin. The test is akin to a short circuit test on a transformer when the secondary side is compromised.

According to Table 1, the design class of the motor affects the empirical ratio of the stator and rotor leakage reactance. However, it is assumed that when the motor class is lacking that.

$X_1 =.$ $X'_2 = 0.5X_{lr}$ is made. The equivalent locked rotor resistance R_{lr} and reactance X_{lr} are calculated as:

$$R_{lr} = \frac{P_{lr}}{3I_{lr}^2} \quad \text{and} \quad X_{lr} = \frac{Q_{lr}}{3I_{lr}^2} \tag{6}$$

The equivalent impedance can be expressed as:

$$Z_{lr} = (R_1 + jX_1) + \{(R'_2 + jX'_2)||JX_m||R_c \tag{7}$$

Since $R'_2 \ll X_m$, Eq. (1) is reduced to:

$$Z_{lr} = \left(R_1 + R'_2\left(\frac{X_m}{X'_2 + X_m}\right)||R_c^2\right)$$
$$+j(X_1 + X'_2\left(\frac{X_m}{X'_2 + X_m}\right)||R_c^2) \tag{8}$$

Since $R_1 + R'_2 \ll R_c$, the value of X'_2 and R'_2 are calculated as:

$$X_2' = (X_{lr} - X_1)\left(\frac{X_m}{X_m + X_1 - X_{lr}}\right) \tag{9}$$

$$R_2' = (R_{lr} - R_1)(\frac{X_2' + X_m}{X_m})^2 \tag{10}$$

2.4 Starting current and starting torque determination

Since the rated voltage and frequency must be delivered to the stator winding when the rotor is locked, the experiments to determine the beginning current and starting torque of IM are virtually destructive. High temperature may be caused by the resultant high current in the stator windings, which may harm the insulation. The rectangular shape of the input impedance Z_1 from the three-phase IM equivalent circuit is provided as follows:

$$Z_1 = R_1 + jX_1 + \left(\frac{Z_2' \times JX_m}{Z_2' + JX_m}\right) \tag{11}$$

where

$$Z_2' = \frac{R_2'}{s} + jX_2' \tag{12}$$

$$I_1 = \frac{V_{phase}}{Z_1} \tag{13}$$

The output torque of an IM is given by

$$T_{mech} = \frac{P_{mech}}{w_{mech}} = \frac{1}{w_{mech}}3I_2'^2\frac{R_2'}{s}(1 - s) = \frac{1}{w_s}3I_2'^2\frac{R_2'}{s} \tag{14}$$

where

$$I_2' = I_1\left(\frac{jX_m}{Z_2' + jX_m}\right) \tag{15}$$

And $\quad w_s = 120f_s/P \quad$ (in rads/s) $\tag{16}$

At starting, $s = 1$, $I_{start} = I_1$ and $T_{start} = T_{mech}$ both estimated at $s = 1$.

2.5 Breakdown torque test

Breakdown torque (T_{max}) is the maximum torque produced by an alternating current motor when the rated voltage is supplied at the rated frequency without causing sudden speed drops. This is sometimes referred to as maximum

torque or pull-out torque [33]. The slip s_{max} values at which the maximum torque T_{max} occurs are as follows:

$$s_{max} = \frac{R_2'}{\sqrt{R_{TH}^2 + \left(X_{TH} + X_2'\right)^2}} \tag{17}$$

While T_{max} is given as:

$$T_{max} = \frac{3V_{TH}^2}{R_{TH} + \sqrt{R_{TH}^2 + \left(X_1 + X_2'\right)^2}} \times \frac{1}{2w_s} \tag{18}$$

where

$$Z_{TH} = R_{TH} + jX_{TH} = \frac{jX_m\left(R_1 + jX_1\right)}{R_1 + j\left(X_1 + X_m\right)} \tag{19}$$

$$V_{TH} = \frac{jX_m}{R_1 + j\left(X_1 + X_m\right)} \times V_\emptyset \tag{20}$$

The rotor resistance R_2' is an important factor in determining the slip at which the greatest torque occurs, as can be shown in Eq. (16). The maximal torque may be deduced from Eq. (17) to be independent of rotor resistance.

3 Simulation result and discussion

The three phase IM equivalent circuit characteristics from the lab tests in [27] and [34] are presented in Table 2 and used as the modeling parameters for the three phase IM in order to verify the correctness of the virtual test.
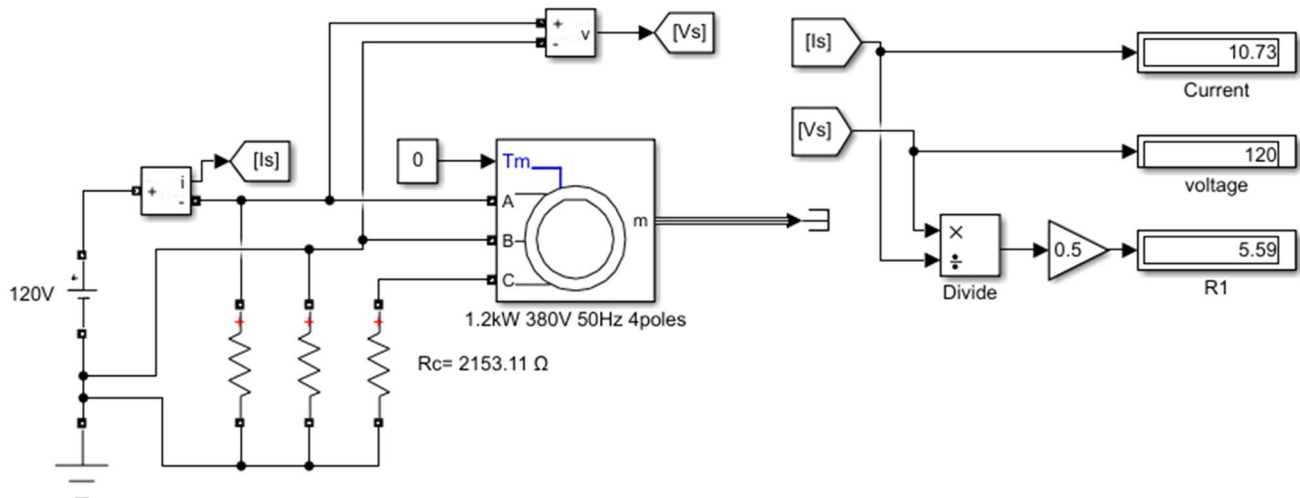
3.1 DC test

A Simulink model is developed, as shown in Fig. 2, to determine the stator resistance R_1 value. The components used in this simulation are the three phase programmable voltage source, the RC load, the permanent magnet synchronous machine, the gain signal, which is used to obtain the desired stator resistance, the three phase programmable voltage source, which converts the Simulink input source to the desired voltage source, and the permanent magnet synchronous machine. The R_1 values for M1 and M2 are shown in Table 3, along with the percentage of accuracy relative to the values used for modeling.

3.1.1 Discussion

As indicated in Table 2, there is a less than 1% difference between the results derived from simulation and those from the laboratory experiment, demonstrating the

Table 2 Squirrel-cage IM parameters obtained from laboratory experiment

Parameters	M1 [27]	M2 [34]
Nominal power	1842.9 VA	5485.3 VA
Voltage and frequency	380 V, 50 Hz	200 V, 60 Hz
Stator (R_1, X_1, L_1)	5.57 Ω, 10.68 Ω, 0.034 H	0.403 Ω, 0.74 Ω, 0.001963 H
Rotor (R_2, X_2, L_2)	4.2 Ω, 10.68, 0.034 H	0.511 Ω, 0.74 Ω, 0.001963 H
Core resistance (R_c)	2153.11 Ω	Not given
X_m, L_m	199.2 Ω, 0.634 H	12.258 Ω, 0.0325 H
Inertia, friction and pole pairs	0.00832 kg.m^2,0.00054 N.m.s/rad, and 2	0.089 kg.m2, 0.0054 N.m.s, and 2

Fig. 2 DC test to determine stator resistance

Table 3 Comparison of DC test simulation result with experiment result

DC test	M1			M2		
	Simulation	Experiment	% Error	Simulation	Experiment	% Error
R_1	5.59 Ω	5.57 Ω	0.36	0.40 Ω	0.403 Ω	0.74

accuracy of this model in performing the test. Real-world DC tests may be carried out using a basic voltmeter-ammeter test or, for small motors, a multimeter. However, since the resistance of big motors is so tiny, a precise instrument is required.

3.2 No-load test

The no-load test is carried out using a Simulink model, and the outcomes of the simulation are shown in Table 4 for both motors. The three-phase measurement is used to show, track, and gauge the power supply's availability. The gain signal amplifies the power supply to kW, the three-phase instantaneous power output from the current and voltage sources signal generates both reactive
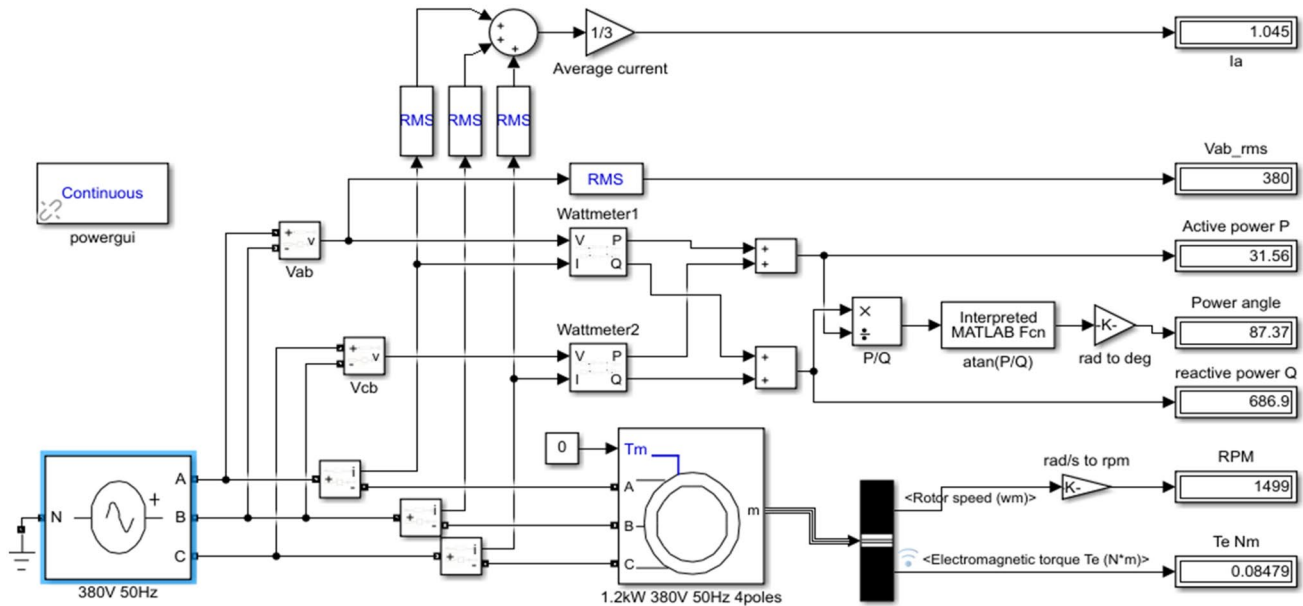
Table 4 No-load test simulation results

No Load Test parameters	M1	M2
Line-line voltage V_{nl}	380 V	200 V
Phase current I_{nl}	1.045 A	8.888 A
3-phase input power P_{nl}	56 W	286.8 W
3-phase input reactive power Q_{nl}	686.9 VAr	3065 VAr
Power angle	87.37^0	84.65^0

and active power, and the three-phase programmable voltage source transforms the Simulink input to the appropriate voltage source. However, the aim of RC loads used in permanent magnet synchronous machines is the same as that of DC tests.

Table 5 Comparison of no-load test simulation result with experiment result

No-load test	M1			M2		
	Simulation	Experiment	% Error	Simulation	Experiment	% Error
R_c	1930 Ω	2153.11 Ω	10	92.84 Ω	NA	NA
X_m	199.5 Ω	199.2 Ω	0.15	12.29 Ω	12.258 Ω	0.26

Fig. 3 Matlab Simulink model for three phase IM No-load test

Using (4) and (5), the following results are obtained:
For M1: $R_c = 1930\,\Omega$ and $X_m = 199.5\,\Omega$.
For M2: $R_c = 92.84\,\Omega$ and $X_m = 12.29\,\Omega$.

Table 5 shows the comparison of the values calculated from no-load simulation results with the values obtained from experiments.

3.2.1 Discussion

There is very little difference between the findings and the experiment values. It should be noted that the core resistance R_c is typically overlooked when the power aspects of IM operation need to be highlighted, which accounts for why the value of R_c is not provided in M2. However, for efficiency calculations, the core losses can be included along with the mechanical losses.

3.3 Locked rotor test

The same modeling used for the IM locked-rotor test as that seen in Fig. 3 is used here. To replicate the locked-rotor scenario, the inertia in the model is adjusted to infinity. Until the line current is reached, the supply voltage is

Table 6 IM Locked-rotor test simulation results

Locked rotor test parameters	M1	M2
Line-line voltage V_{lr}	110.9 V	46.19
Phase current I_{lr}	2.8A	15.8
3-phase input power P_{lr}	219.8	641.2
3-phase input reactive power Q_{lr}	491.3	1090
Power angle ($\cos^{-1} PF$)	65.9^0	59.54

changed. Table 6 displays the results of the simulation for a locked rotor.

By using (6), (9) and (10), the following results are obtained for M1: $X_2' = 10.72\,\Omega$ and $R_2' = 4.19\,\Omega$ while for M2: $X_2' = 0.73\,\Omega$ and $R_2' = 0.509\Omega$ Table 7 shows the comparison of the values calculated from simulation results with the values obtained from experiments.

3.3.1 Discussion

Table 7 shows that, for the locked rotor test, the model's accuracy is shown by the simulation results and experiment parameters being quite similar.

3.4 Starting current and starting torque determination

The simulation to determine I_{start} and T_{start} is accomplished by setting the inertia to infinity so that the rotor is locked. I_{start} and T_{start} are then obtained at the nominal voltage and frequency. While the motor is at stall, the starting current obtained for M1 (Fig. 4) is 13.6 A with the rms value at the fundamental frequency being $\frac{13.6}{\sqrt{2}} = 9.6A$. The electromagnetic torque (Fig. 5) settles at 6.6 Nm following the initial

oscillations. I_{start} and T_{start} for M2 are obtained as 68.37 A and 33.66 Nm.

3.4.1 Discussion

Theoretical values of I_{start} and T_{start} are derived by using (11–16) with s = 1 and are then contrasted with the results of the simulation; the comparison is presented in Table 8. The table shows that there is very little fference between the simulation result and values from the theoretical formula.

Table 7 Comparison of locked rotor test simulation result with experiment result

Locked rotor test	M1			M2		
	Simulation	Experiment	% Error	Simulation	Experiment	% Error
X_1	10.72 Ω	10.68 Ω	0.37	0.73 Ω	0.74 Ω	1.35
X_2'	10.72 Ω	10.68 Ω	0.37	0.73 Ω	0.74 Ω	1.35
R_2'	4.19 Ω	4.20 Ω	0.24	0.509 Ω	0.511 Ω	0.39
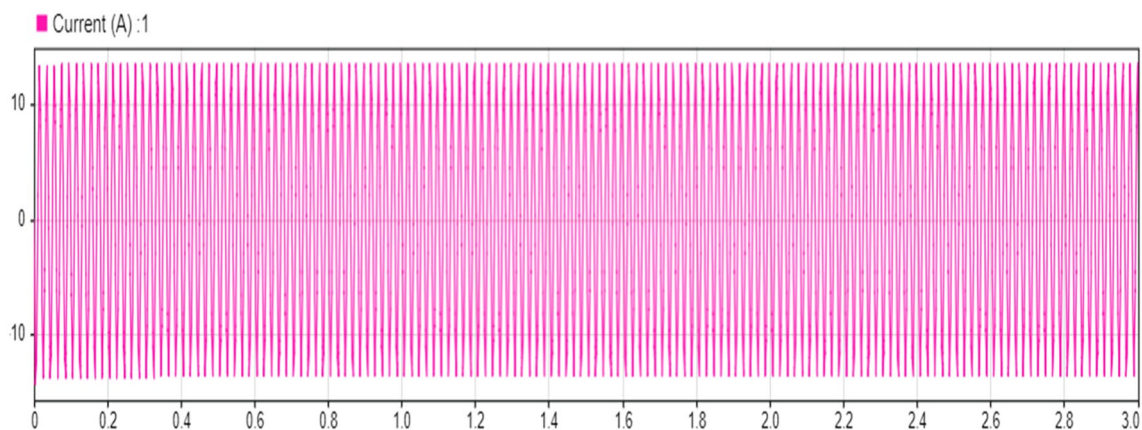
Fig. 4 Starting current (A) versus time (s)
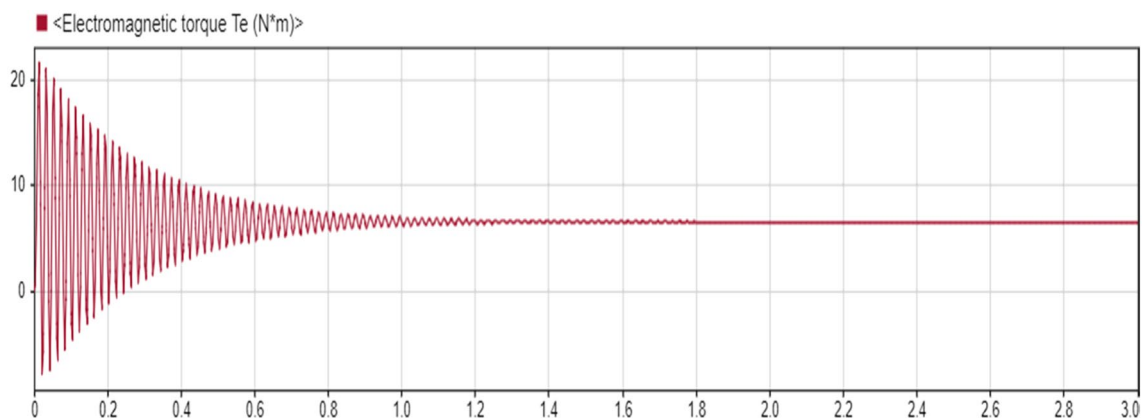
Fig. 5 Electromagnetic torque (Nm) versus time (s)

3.5 Breakdown torque determination

The breakdown torque test is performed by starting the motor at the rated voltage and frequency up to steady state. The ramp signal is used to increase the load torque by ramping up the ramp slope appropriately (4 Nm in this case). An initial delay period of 1 s was selected so that the motor could attain steady condition before the load was applied. As the load torque increases, the speed drops, electromagnetic torque increases, and stator line current increases. When the load torque hits T_{max}, the electromagnetic torque and speed rapidly decrease to zero, while the stator current quickly increases back to its previous value. At a maximum slip s max of 0.1923, motor M1 generated a maximum induced torque T_{max}, of 15.58 Nm (Fig. 6). T max for motor M2 was 50.94 Nm, and s_{max} was 0.3511.

3.5.1 Discussion

By applying (17).and (18), theoretical values of s_{max} and T_{max} are obtained and compared with the simulation outputs. The comparison is shown in Table 9.

When the T_{max} acquired by simulation is contrasted with the theoretical value, a variance of 0.06% in M1 and a variation of 0.3% in M2 are found. In both motors, the error in the slip value at which the maximum torque occurs is just 0.9%. These results demonstrate that a virtual test design may be used to more accurately predict the breakdown torque test. The values obtained from simulation and the experiment parameters are used to obtain the torque speed characteristics shown in Fig. 7

3.6 Torque-speed and current-speed characteristics

The torque-speed and current-speed characteristics of both motors are obtained using the appropriate MATLAB code, and they are shown in Fig. 8 for comparison. The results of the prior computations are supported by the plot of the two attributes.

3.7 Effect of varying the rotor resistance

Rotor resistance has an influence on the slip value at which the torque reaches its maximum, but it has no effect on the breakdown torque T_{max}. Consequently, the slip value
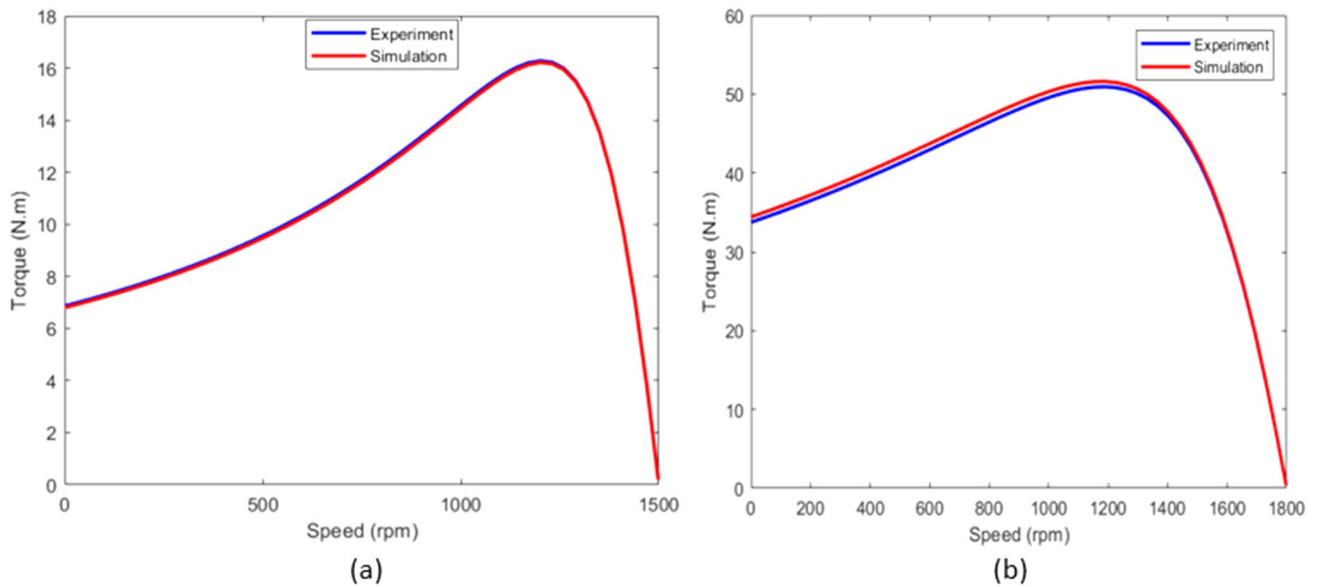
Table 8 Comparison of I_{start} and T_{start} from simulation with theoretical values

Starting current and torque	M1			M2		
	Simulation	Theoretical	% Error	Simulation	Theoretical	% Error
I_{start}	9.6 A	9.58	0.21	68.37	68.3	0.1
T_{start}	6.6 A	6.63	0.45	33.66	33.8	0.4
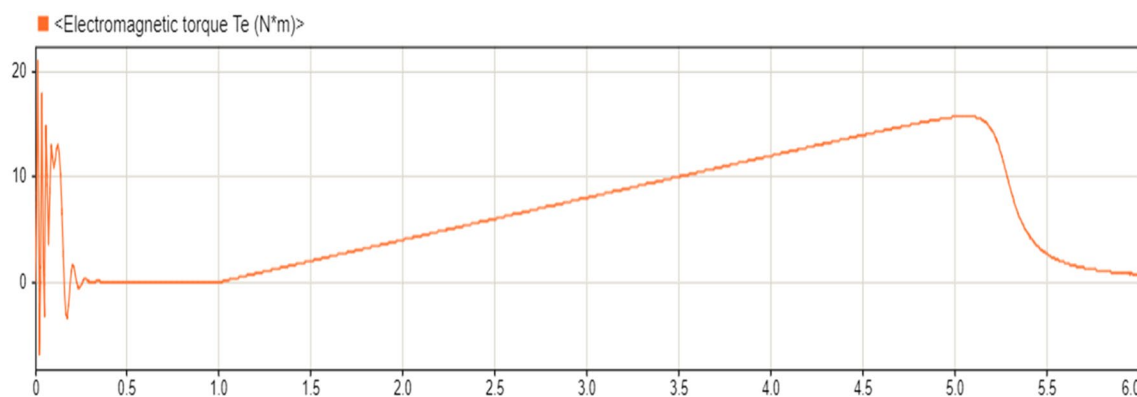
Fig. 6 Breakdown torque (Nm) versus time (s) for motor M1

Table 9 Comparison of s_{max} and T_{start} from simulation with theoretical values

Breakdown torque test	M1			M2		
	Simulation	Theoretical	% Error	Simulation	Theoretical	% Error
s_{max}	0.1923	0.195	0.87	0.351	0.348	0.9
T_{max}	15.58 Nm	15.59	0.06	50.94	51.1	0.3

Fig. 7 Torque-speed cracteristics using experiment parameters and simulation parameters **a** M1, **b** M2
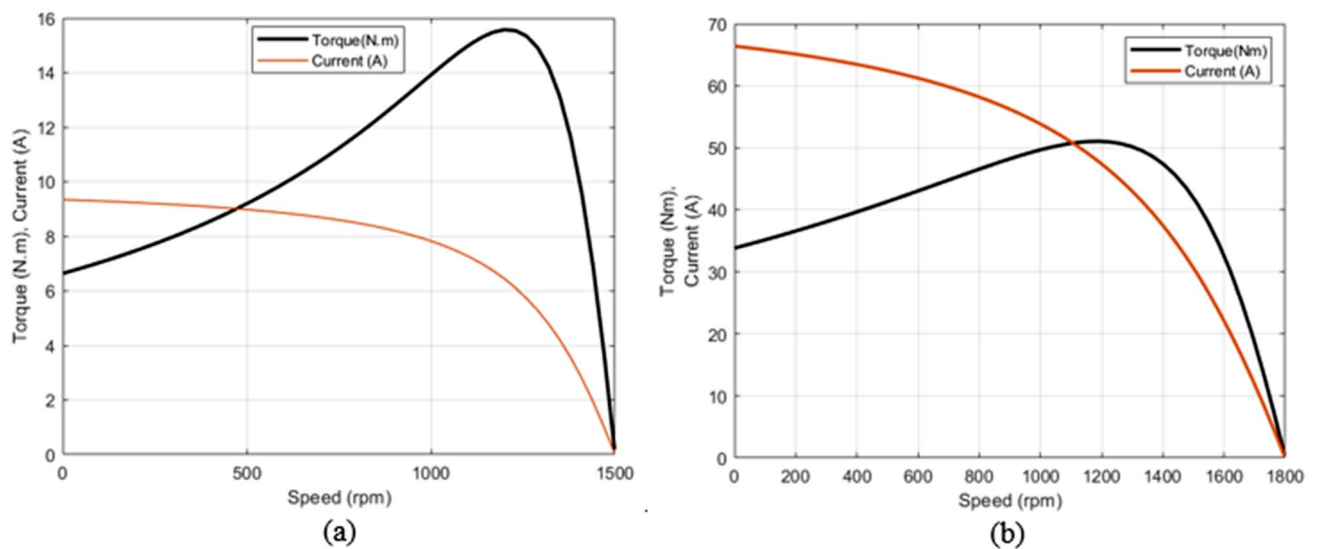

Fig. 8 Torque (Nm), Input current (A) against rotor speed (rpm) for **a** M1 **b** M2

at which the peak torque occurs rises as rotor resistance increases. As a result, when a high starting torque is required, the rotor resistance value is carefully selected to provide T_{max} at rest. Such a design must have a s_{max} of 1.00. For motor M1, for instance, using (17) and (19):

$$Z_{TH} = R_{TH} + jX_{TH} = \frac{jX_m(R_1 + jX_1)}{R_1 + j(X_1 + X_m)} = \frac{j199.2(5.57 + j10.68)}{5.57 + j(10.68 + 199.2)} = 5.014 + j10.27$$

$$s_{max} = \frac{R'_2}{\sqrt{R_{TH}^2 + \left(X_{TH} + X'_2\right)^2}};$$

$$1 = \frac{R'_2}{\sqrt{5.014^2 + (10.27 + 10.68)^2}} = \frac{R'_2}{21.542} \quad \therefore R'_2 = 21.542 \ \Omega$$

Therefore, for motor M1, an additional 17.342 must be added to the 4.2 to get maximum torque at startup. Similar calculations may be made for motor M2 to determine that 1.493 is necessary for the maximum torque to occur at startup. When $R'_2 = 21.542$ for M1 and 1.493 for M2, Fig. 9 displays the torque-speed characteristics for both motors. It should be noted that the beginning current decreases in all scenarios as a result of the increased rotor resistance, which is preferable for a low starting current and a high starting power factor. However, raising R'_2 caused a significant slip during routine operation, which increased rotor losses and decreased efficiency. Due of this contradictory need, wound-rotor IM uses external rotor resistance to meet both criteria during startup and regular operation.

3.8 Effect of varying R'_2

Figure 10a, b, respectively, demonstrate how the R'_2 of M1 and M2 is altered. It has been shown that as rotor resistance rises, so does the slip at which the highest torque occurs, indicating that the motor's peak torque is reached at a lower speed. However, the peak torque values of 15.6 Nm (M1) and 50.9 Nm (M2) did not change.
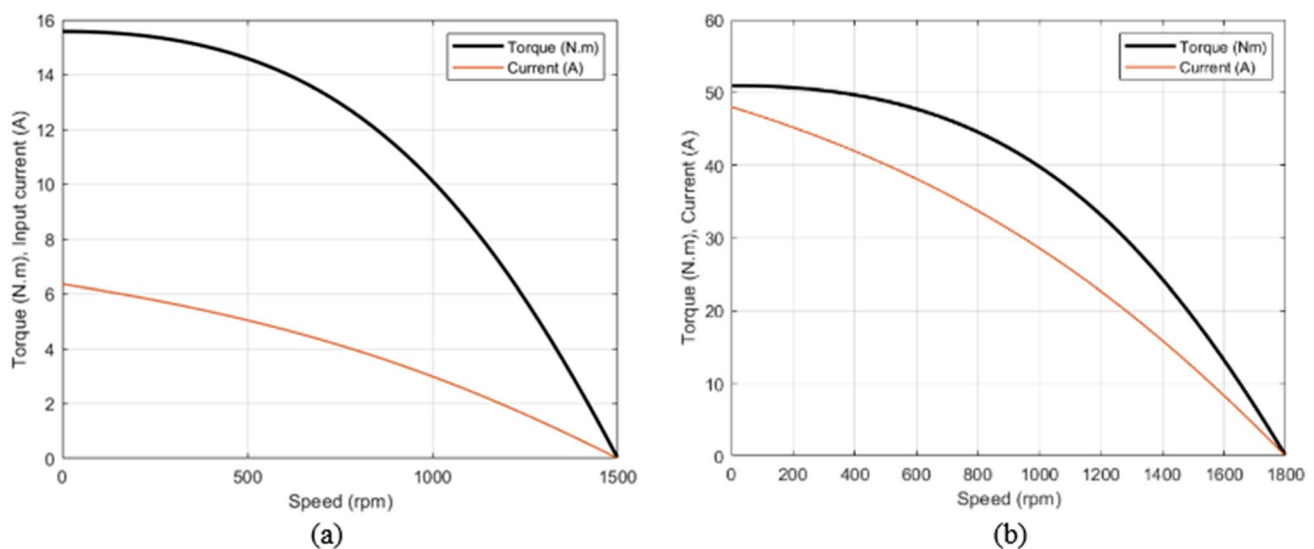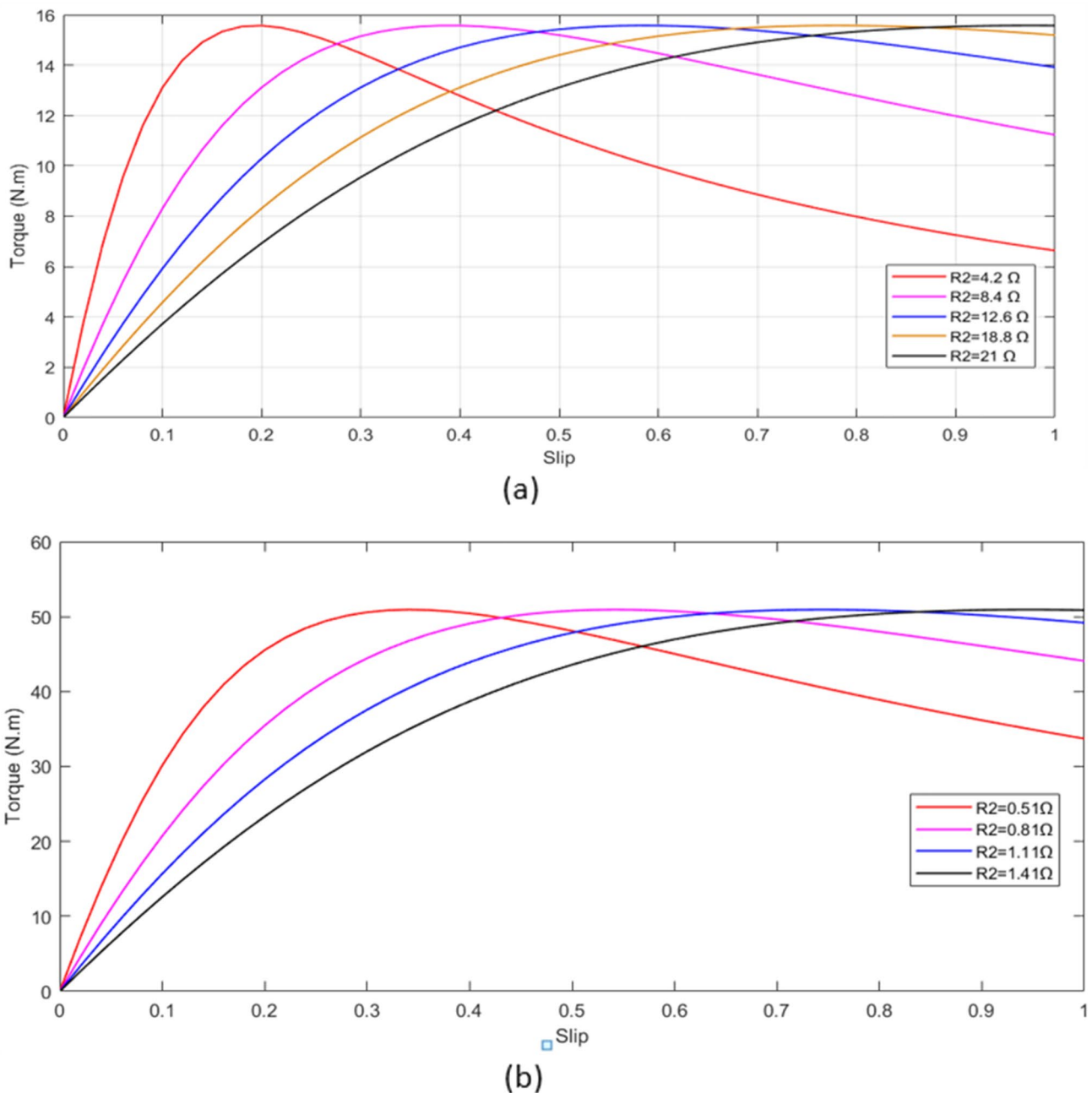
4 Conclusions and recommendations

In this paper, several virtual experiments on induction motors are performed with improved precision using simulation models. The tests include the basic tests to determine the per-phase equivalent circuit of induction motors which are the dc test, no-load test and the locked rotor tests. Others are the torque-speed and current-speed characteristics tests as well as performance features like the starting current and starting torque determination tests. In contrast to actual studies, this kind of virtual testing saves time and prevents the threat of harming electrical equipment via risky tests like load testing and breakdown torque determination tests. The techniques used in this study are straightforward and simple to utilize, even for those with just a basic grasp of MATALAB/Simulink. They also provide far more flexibility, enhanced accuracy, and a better comprehension of both the observations and the outcomes.

In the no-load test which is used to determine the core loss resistance Rc and the magnetizing reactance Xm in the IM per-phase equivalent circuit, a discrepancy of 10% is evaluated between the model result and the result from the laboratory. This is quite significant, and a more efficient model needs to be researched to reduce the error to a reasonably lesser value. In [34], Rc is neglected which is usually the case when the power aspects of IM operation is being emphasized. However, for efficiency calculations, the core losses has to be included along with the mechanical losses. This can be incorporated in the future

Fig. 9 Torque-speed characteristics for Motors M1 and M2 at calculated values of R'_2. for maximum starting torque

Fig. 10 Torque-speed characteristics at different rotor resistance of **a** M1, **b** M2

research. Furthermore, a similar study can be carried out to develop models which can be used to study other types of electric motors such as the permanent magnet DC motors and switched reluctance motors which are also relevant in many modern applications such as in electric vehicle.

Lastly, the authors acknowledge that the MATLAB Simulink model developed in this study can often be appropriate for conducting tests on induction motors, but in some cases, it cannot completely replace the experimental work. Hence, experimental studies should go hand in hand with the computer models.

Declarations

Conflict of interest The authors have no relevant financial or non-financial interests to disclose.

Ethical approval This article does not contain any studies with human participants or animals performed by any of the authors.

References

1. Diallo D, Benbouzid MEH, Makouf A (2004) A fault-tolerant control architecture for induction motor drives in automotive applications. IEEE Trans Veh Technol 53(6):1847–1855. https://doi.org/10.1109/TVT.2004.833610

2. Chen L et al (2014) A high-performance control method of constant-controlled induction motor drives for electric vehicles. Math Probl Eng. https://doi.org/10.1155/2014/386174

3. Esen GK, Özdemir E (2017) A new field test method for determining energy efficiency of induction motor. IEEE Trans Instrum Meas 66(12):3170–3179. https://doi.org/10.1109/TIM.2017.2735718

4. Wang K et al (2019) Comparison study of induction motor models considering iron loss for electric drives. Energies 12(3):503. https://doi.org/10.3390/en12030503

5. Fathy Abouzeid A et al (2020) Control strategies for induction motors in railway traction applications. Energies 13(3):700. https://doi.org/10.3390/en13030700

6. Kazakbaev V et al (2019) Efficiency analysis of low electric power drives employing induction and synchronous reluctance motors in pump applications. Energies 12(6):1144. https://doi.org/10.3390/en12061144

7. Aziri H, et al. (2017) Simulation of three-phase induction motor drives using indirect field oriented control in PSIM environment. In: AIP Conference Proceedings. 2017, AIP Publishing LLC. https://doi.org/10.1063/1.5002063

8. Albalawi H, Zaid SA, Buswig YM (2019) Simulation study of two torque optimization methods for direct torque-controlled induction motors. Appl Sci 9(24):5547. https://doi.org/10.3390/app9245547

9. Dems M et al (2021) Dynamic simulation of high-speed induction motor. Energies 14(9):2713. https://doi.org/10.3390/en14092713

10. Paramo-Balsa P et al (2021) A low-cost non-intrusive method for in-field motor speed measurement based on a smartphone. Sensors 21(13):4317. https://doi.org/10.3390/s21134317

11. Diab AAZ et al (2019) Robust speed controller design using H_infinity theory for high-performance sensorless induction motor drives. Energies 12(5):961. https://doi.org/10.3390/en12050961

12. Karlovsky P, Lettl J (2018) Induction motor drive direct torque control and predictive torque control comparison based on switching pattern analysis. Energies 11(7):1793. https://doi.org/10.3390/en11071793

13. Gonzalez O et al (2019) Predictive-fixed switching current control strategy applied to six-phase induction machine. Energies 12(12):2294. https://doi.org/10.3390/en12122294

14. Dybkowski M, Bednarz SA (2019) Modified rotor flux estimators for stator-fault-tolerant vector controlled induction motor drives. Energies 12(17):3232. https://doi.org/10.3390/en12173232

15. Kali Y et al (2019) Current control of a six-phase induction machine drive based on discrete-time sliding mode with time delay estimation. Energies 12(1):170. https://doi.org/10.3390/en12010170

16. Fedor P et al (2021) New stable non-vector control structure for induction motor drive. Appl Sci 11(14):6518. https://doi.org/10.3390/en12010170

17. Che HS et al (2013) Postfault operation of an asymmetrical six-phase induction machine with single and two isolated neutral points. IEEE Trans Power Electron 29(10):5406–5416. https://doi.org/10.1109/TPEL.2013.2293195

18. Mirzaeva G et al (2016) A generalized MPC framework for the design and comparison of VSI current controllers. IEEE Trans Industr Electron 63(9):5816–5826. https://doi.org/10.1109/TIE.2016.2578283

19. Zhang Z et al (2021) Ripple attenuation for induction motor finite control set model predictive torque control using novel fuzzy adaptive techniques. Processes 9(4):710. https://doi.org/10.3390/pr9040710

20. Rosa FC, Bim E (2020) A constrained non-linear model predictive controller for the rotor flux-oriented control of an induction motor drive. Energies 13(15):3899. https://doi.org/10.3390/en13153899

21. Lipcak O et al (2021) Current ripple reduction of predictive torque-controlled induction motor drive using delta-star switchover. Appl Sci 11(6):2863. https://doi.org/10.3390/app11062863

22. Bao D et al (2018) Sensorless speed control based on the improved Q-MRAS method for induction motor drives. Energies 11(1):235. https://doi.org/10.3390/en11010235

23. Golsorkhi MS, Binandeh H, Savaghebi M (2021) Online efficiency optimization and speed sensorless control of single-phase induction motors. Appl Sci 11(19):8863. https://doi.org/10.3390/app11198863

24. Fnaiech MA et al (2021) MRAS-based switching linear feedback strategy for sensorless speed control of induction motor drives. Energies 14(11):3083. https://doi.org/10.3390/en14113083

25. Kuchar M et al (2021) Self-tuning observer for sensor fault-tolerant control of induction motor drive. Energies 14(9):2564. https://doi.org/10.3390/en14092564

26. Gonzalez-Prieto A et al (2020) Automatic fault-tolerant control of multiphase induction machines: a game changer. Electronics 9(6):938. https://doi.org/10.3390/electronics9060938

27. Bentounsi A et al (2010) Computer-aided teaching using MATLAB/Simulink for enhancing an IM course with laboratory tests. IEEE Trans Educ 54(3):479–491. https://doi.org/10.1109/TE.2010.2085046

28. Bharatiraja C et al (2017) Design and implementation of fourth arm for elimination of bearing current in NPC-MLI-Fed induction

motor drive. IEEE Trans Ind Appl 54(1):745–754. https://doi.org/10.1109/TIA.2017.2759204

29. Sengamalai U et al (2022) Three phase induction motor drive: a systematic review on dynamic modeling, parameter estimation, and control schemes. Energies 15(21):8260. https://doi.org/10.3390/en15218260

30. Nguyen TD, Lee H-H (2011) Modulation strategies to reduce common-mode voltage for indirect matrix converters. IEEE Trans Industr Electron 59(1):129–140. https://doi.org/10.1109/TIE.2011.2141101

31. Lee S-H et al (2017) Identification of induction motor parameters at standstill based on integral calculation. IEEE Trans Ind Appl 53(3):2130–2139. https://doi.org/10.1109/TIA.2017.2650141

32. Srndovic M, Fišer R, Grandi G (2019) Analysis of equivalent inductance of three-phase induction motors in the switching frequency range. Electronics 8(2):120. https://doi.org/10.3390/electronics8020120

33. Casadei D, et al. (2005) A robust method for flux weakening operation of DTC induction motor drive with on-line estimation of the break-down torque. In: 2005 European Conference on Power Electronics and Applications, IEEE. https://doi.org/10.1109/EPE.2005.219305

34. Ayasun S, Nwankpa CO (2005) Induction motor tests using MATLAB/Simulink and their integration into undergraduate electric machinery courses. IEEE Trans Educ 48(1):37–46. https://doi.org/10.1109/TE.2004.832885